ELSEVIER

www.elsevier.nl/locate/jorganchem

Journal of Organometallic Chemistry 616 (2000) 54–66

Journal of Organometallic Chemistry

Synthesis, crystal structure, and reactions of the 17-valence-electron rhenium methyl complex $[(\eta^5\text{-}C_5Me_5)Re(NO)(P(4\text{-}C_6H_4CH_3)_3)(CH_3)]^{\bullet+}$ $B(3,5\text{-}C_6H_3(CF_3)_2)_4^-$: experimental and computational bonding comparisons with 18-electron methyl and methylidene complexes

Jean Le Bras [a], Haijun Jiao [a], Wayne E. Meyer [b], Frank Hampel [a], J.A. Gladysz [a,*]

[a] *Institut für Organische Chemie, Friedrich-Alexander Universität Erlangen-Nürnberg, Henkestrasse 42, 91054 Erlangen, Germany*
[b] *Department of Chemistry, University of Utah, Salt Lake City, UT 84112, USA*

Received 23 June 2000

Abstract

Reactions of methyl complex $(\eta^5\text{-}C_5Me_5)Re(NO)(P(4\text{-}C_6H_4CH_3)_3)(CH_3)$ (**2b**) and the ferrocenium salt $(\eta^5\text{-}C_5H_5)_2Fe^{\bullet+}$ BAr_F^- ($BAr_F^- = B(3,5\text{-}C_6H_3(CF_3)_2)_4^-$) or the trityl salt Ph_3C^+ BAr_F^- give the very air sensitive title radical cation $\mathbf{2b}^{\bullet+}$ BAr_F^- or the robust methylidene complex $[(\eta^5\text{-}C_5Me_5)Re(NO)(P(4\text{-}C_6H_4CH_3)_3)(=CH_2)]^+$ BAr_F^- ($\mathbf{3b}^+$ BAr_F^-) as analytically pure powders in 80% yields. The crystal structures of **2b** and $\mathbf{2b}^{\bullet+}$ BAr_F^- are determined. With the aid of high level density functional calculations on model complexes, key structural, bonding, and dynamic properties are compared. Similar quantities are calculated for $\mathbf{3b}^+$ BAr_F^-, which could not be crystallized, and the $Re{=}CH_2$ rotational barrier is bounded by NMR ($\Delta G^{\ddagger}_{383\ K} > 17.5$ kcal mol^{-1}). Special attention is given to structural manifestations of backbonding, particularly with the phosphine ligands. Cobaltocene and $\mathbf{2b}^{\bullet+}$ BAr_F^- react to give **2b**. However, no phosphine exchange or well-defined thermal decomposition products of $\mathbf{2b}^{\bullet+}$ BAr_F^- are detected.

Keywords: Rhenium; Radical cation; 'Barf' anion; Methylidene complex; Density functional calculation

1. Introduction

Organometallic complexes with 17 valence electrons have numerous important physical and chemical properties that are not shared by their 18 and 16-valence-electron counterparts [1]. However, for a variety of reasons — in some cases their low thermal stability or high chemical reactivity, and in other cases the restricted utility of NMR for characterization — they remain far less studied. One specific major class would be cyclopentadienyl 'piano stool' complexes of the formula $(\eta^5\text{-}C_5R_5)M(L)(L')(L'')$ [1–3], for which cationic, neutral, and anionic radicals have been observed and in a few cases isolated [4,5].

As described in the preceding paper [6], we have had a special interest in complexes where sp carbon chains bridge two transition metals, and their properties as a function of redox state [7]. The dirhenium C_4 radical cation $[(\eta^5\text{-}C_5Me_5)Re(NO)(P(C_6H_5)_3)(CCCC)((C_6H_5)_3P)(ON)Re(\eta^5\text{-}C_5Me_5)]^{\bullet+}$ PF_6^- ($\mathbf{1}^{\bullet+}$ PF_6^-) is isolable, and the odd electron (and positive charge) is delocalized between the two rheniums on the rapid IR and ESR time scales [7b]. Thus, we have sought to rigorously characterize similar monorhenium radical cations, in which the metal would carry higher spin density and a full formal positive charge. Accordingly, oxidations of methyl complexes $(\eta^5\text{-}C_5Me_5)Re(NO)(PR_3)(CH_3)$ (**2**) to spectroscopically observable radical cations $[(\eta^5\text{-}C_5Me_5)Re(NO)(PR_3)(CH_3)]^{\bullet+}$ X^- ($\mathbf{2}^{\bullet+}$ X^-; $X^- = PF_6^-$, SbF_6^-) that persist for hours in solution at room tem-

* Corresponding author. Tel.: +49-9131-8522540; fax: +49-9131-8526865.
E-mail address: gladysz@organik.uni-erlangen.de (J.A. Gladysz).

0022-328X/00/$ - see front matter
PII: S0022-328X(00)00531-3

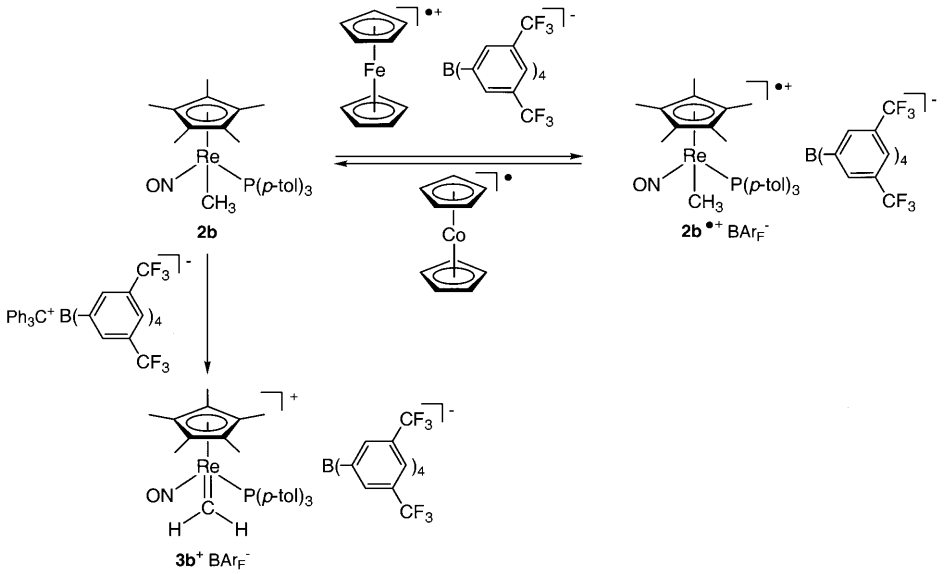

Scheme 1. Synthesis of new complexes.

perature are detailed in the preceding paper [6]. Phosphine ligands that are more electron rich and/or bulkier than triphenylphosphine were found to be advantageous.

In the course of these efforts, we discovered that further optimization of the anion allowed one such radical cation to be isolated in crystalline form. In this paper, we report the synthesis and structural characterization of the 'barf' salt of the tri(*p*-tolyl)phosphine complex $[(\eta^5\text{-}C_5Me_5)Re(NO)(P(4\text{-}C_6H_4CH_3)_3)(CH_3)]^{\bullet+}$ BAr_F^- (**2b**$^{\bullet+}$ BAr_F^-) [8]. The rationale for a separate publication is to facilitate comparisons of this scarce class of compound [4] with 18-valence-electron congeners. Towards this end, we also describe: (1) the crystal structure of the precursor methyl complex **2b**; (2) the isolation and spectroscopic characterization of the corresponding methylidene complex $[(\eta^5\text{-}C_5Me_5)Re(NO)(P(4\text{-}C_6H_4CH_3)_3)(=CH_2)]^+$ BAr_F^- (**3b**$^+$ BAr_F^-); and (3) supporting high-level density functional calculations on models for all of these compounds. The latter allow a more precise analysis of structural, bonding, and dynamic properties.

2. Results

2.1. The title radical cation

As exemplified by recent successes involving organorhenium cations [9], BAr_F^- is increasingly being recognized as a 'stability-conferring' anion. Possible favorable factors include its large size, and the presence of aryl rings that can promote crystallinity. However, it is not totally innocent [10]. In the previous paper, we found that the ferrocenium cation readily oxidized methyl complexes **2** [6]. Accordingly, the previously reported [9b,11] salt $(\eta^5\text{-}C_5H_5)_2Fe^{\bullet+}$ BAr_F^- was prepared in 80% yield by a standard procedure.

As shown in Scheme 1, the tri(*p*-tolyl)phosphine methyl complex **2b** [6] and $(\eta^5\text{-}C_5H_5)_2Fe^{\bullet+}$ BAr_F^- were combined in CH_2Cl_2 at room temperature. Workup gave a tan powder with properties consistent for the radical cation **2b**$^{\bullet+}$ BAr_F^- in 80% yield. When the educts were not of the highest purities, much lower yields were obtained. Complex **2b**$^{\bullet+}$ BAr_F^- was very air sensitive both in solution and the solid state, and all measurements utilized freshly prepared samples. Microanalyses (C–H–N) were only marginally satisfactory. However, the IR spectrum showed a strong ν_{NO} band at 1714 cm^{-1}, in agreement with the much less stable **2b**$^{\bullet+}$ PF_6^- [6]. The ESR spectrum was similar to those of other **2**$^{\bullet+}$ X^- salts [6], as depicted in Fig. 1. As expected, no NMR signals were detected. A cyclic voltammogram showed a reversible one electron reduction, and was equivalent to that of the precursor **2b**.

Prisms of **2b**$^{\bullet+}$ BAr_F^- were readily and reproducibly obtained from CH_2Cl_2–hexane. The crystal structure was determined as outlined in Table 1 and in Section 4. Fig. 2 (bottom) confirms the proposed formulation, and

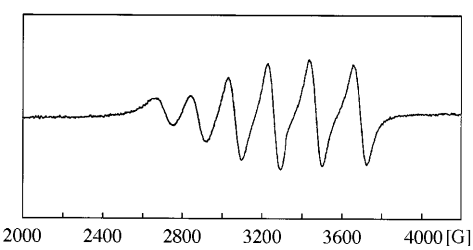

Fig. 1. ESR spectrum of **2b**$^{\bullet+}$ BAr_F^-.

Table 1
Crystallographic data for **2b** and **2b**$^{\bullet+}$ BAr_F^- [a]

Complex	**2b**	**2b**$^{\bullet+}$ BAr_F^-
Empirical formula	$C_{32}H_{39}NOPRe$	$C_{64}H_{51}BF_{24}NOPRe$
Formula weight	670.81	1534.04
Temperature (K)	173(2)	173(2)
Wavelength (Å)	0.71073	0.71073
Crystal system	Monoclinic	Monoclinic
Space group	$P2_1/c$	$P2_1/n$
Cell dimensions		
a (Å)	8.5697(10)	12.526(3)
b (Å)	19.787(2)	14.900(3)
c (Å)	16.864(3)	34.288(7)
β (°)	93.346(11)	97.92(3)
V (Å^3)	2854.7(6)	6338(2)
Z	4	4
D_{calc} (g cm^{-3})	1.561	1.608
Absorption coefficient (mm^{-1})	4.337	2.056
F(000)	1344	3044
Crystal size (mm^3)	$0.30\times0.30\times0.20$	$0.40\times0.40\times0.40$
θ limit (°)	2.38–26.28	2.60–25.01
Index ranges	$10\le h\le10$, $-24\le k\le0$, $-21\le l\le0$	$0\le h\le14$, $0\le k\le17$, $-40\le l\le40$
Reflections collected	5987	11673
Independent reflections	5788 [$R_{int}=0.0709$]	11124 [$R_{int}=0.0622$]
Reflections [$I>2\sigma(I)$]	3918	6010
Data/restraints/parameters	5788/0/325	11124/0/838
Goodness-of-fit on F^2	1.031	1.017
Final R indices [$I>2\sigma(I)$]	$R_1=0.0494$, $wR_2=0.0949$	$R_1=0.0700$, $wR_2=0.1362$
R indices (all data)	$R_1=0.0912$, $wR_2=0.1115$	$R_1=0.1508$, $wR_2=0.1730$
Δp (max), (e Å^{-3})	2.272 and −0.855	1.135 and −0.700

[a] $R=\Sigma(||F_o|-|F_c||)/\Sigma(|F_o|)$; $R_w=[\Sigma(w(|F_o|-|F_c|^2/\Sigma(w|F_o|^2)]^{1/2}$.

Table 2 lists key bond lengths and angles. Atomic coordinates and other data have been deposited in the Cambridge Crystallographic database. In accord with much precedent, the rhenium is formally octahedral, with C–Re–P, C–Re–N, and P–Re–N bond angles close to 90°. One consequence (important below) is that the methyl ligand cannot adopt a perfectly staggered or eclipsed conformation with respect to rhenium and the three other ligands. This requires two tetrahedral atoms, as in ethane. Additional structural features are analyzed in conjunction with the computational data.

Fundamental chemical properties of **2b**$^{\bullet+}$ BAr_F^- were explored. First, as shown in Scheme 1, reduction with cobaltocene, $(\eta^5\text{-}C_5H_5)_2Co^{\bullet}$, gave the precursor methyl complex **2b** in 90% yield after workup. Second, **2b**$^{\bullet+}$ BAr_F^- and triphenylphosphine, $P(C_6H_5)_3$ (five equivalents), were combined in CH_2Cl_2 at 22°C. After 1 h, cobaltocene was added. Workup gave only **2b**. None of the previously characterized substitution product $(\eta^5\text{-}C_5Me_5)Re(NO)(P(C_6H_5)_3)(CH_3)$ (**2a**) [6,13] was detected. Third, isolated samples of **2b** and **2b**$^{\bullet+}$ BAr_F^-

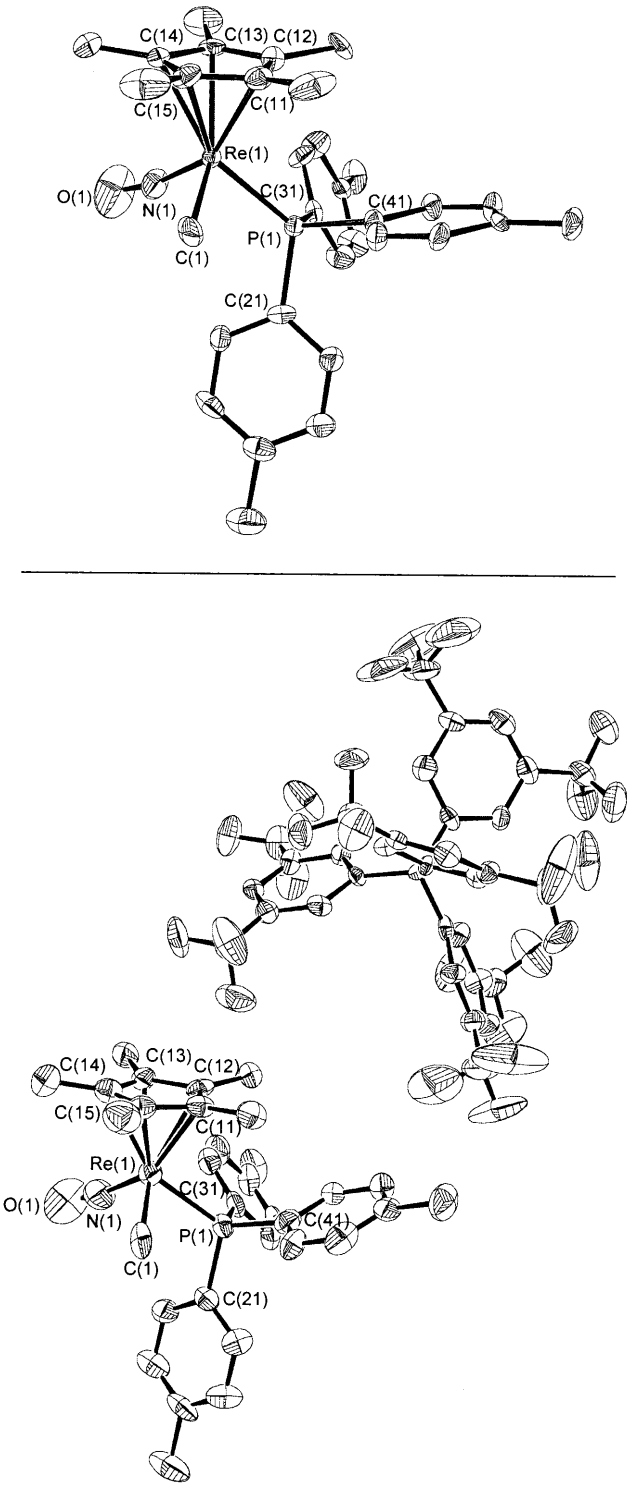

Fig. 2. Molecular structure of complexes **2b** (top) and **2b**$^{\bullet+}$ BAr_F^- (bottom).

Table 2
Key distances (Å) and angles (°) in **2b** and **2b**$^{\bullet+}$ BAr_F^-

	2b	**2b**$^{\bullet+}$ BAr_F^-
Bond lengths		
Re(1)–C(1)	2.123(11)	2.120(12)
Re(1)–P(1)	2.359(2)	2.455(3)
Re(1)–N(1)	1.787(9)	1.813(12)
N(1)–O(1)	1.175(11)	1.027(13)
P(1)–C(21)	1.825(8)	1.827(11)
P(1)–C(31)	1.829(9)	1.811(11)
P(1)–C(41)	1.839(9)	1.805(12)
Re(1)–Cp* (centroid)	1.970(9)	1.985(11)
Bond angles		
C(1)–Re(1)–P(1)	88.1(3)	89.8(3)
C(1)–Re(1)–N(1)	97.9(5)	99.7(5)
P(1)–Re(1)–N(1)	92.7(3)	91.8(4)
O(1)–N(1)–Re(1)	169.4(9)	169.4(14)
C(21)–P(1)–Re(1)	119.3(3)	113.8(4)
C(31)–P(1)–Re(1)	116.3(3)	115.3(4)
C(41)–P(1)–Re(1)	113.2(3)	109.6(4)

were combined in a 95:5 ratio in CH_2Cl_2. After 10 min, a more basic triarylphosphine, P(4-$C_6H_4OMe)_3$ (five equivalents), was added. The sample was worked up after 1 h. A ^{1}H-NMR spectrum (C_6D_6) showed only **2b**, and none of the known complex (η^5-C_5Me_5)Re(NO)(P(4-$C_6H_4OMe)_3$)(CH_3) (**2e**) [6]. Other related attempts to effect phosphine substitution were also unsuccessful.

Finally, **2b**$^{\bullet+}$ BAr_F^- was dissolved in CD_3CN at −78°C and slowly warmed to room temperature. Under analogous conditions, the markedly less stable cyclopentadienyl radical cation [(η^5-C_5H_5)Re(NO)(P($C_6H_5)_3$)(CH_3)]$^{\bullet+}$ X^- (**4a**$^{\bullet+}$ X^-) undergoes clean bimolecular decomposition to a 1:1:1 mixture of a methylidene complex, an acetonitrile complex, and methane, as shown in Scheme 2 [12]. A ^{1}H-NMR spectrum showed many new C_5Me_5 signals, but no low field resonances. An IR spectrum showed a ν_{NO} band at 1633 cm^{-1}, suggestive of neutral 18-valence-electron products. No gas evolution was observed. Hence, the bulkier pentamethylcyclopentadienyl ligand in **2b**$^{\bullet+}$ BAr_F^- appears to block analogous chemistry.

2.2. Related complexes

As previously reported [13], reaction of the triphenylphosphine methyl complex **2a** and trityl hexafluorophosphate, Ph_3C^+ PF_6^-, gives the stable methylidene complex [(η^5-C_5Me_5)Re(NO)(P($C_6H_5)_3$)(=CH_2)]$^+$ PF_6^- (**3a**$^+$ PF_6^-) [14]. However, the crystal structure shows severe nitrosyl–methylidene ligand positional disorder [13]. We sought to synthesize the corresponding tri(*p*-tolyl)phosphine methylidene complex **3b**$^+$ X^- by a similar method, and obtain better structural data if possible. One of several objectives was to be certain that the crystals represented above as **2b**$^{\bullet+}$ BAr_F^- were not in fact **3b**$^+$ BAr_F^-. These complexes differ by only a hydrogen atom, and would be very difficult to distinguish crystallographically.

As shown in Scheme 1, **2b** and the known trityl 'barf' salt, Ph_3C^+ BAr_F^- [15], were reacted. Workup gave the methylidene complex **3b**$^+$ BAr_F^- as an analytically pure yellow powder in 80% yield. The ^{1}H-NMR spectrum showed two diagnostic low field =CH_2 signals (δ 15.17, 14.22, CD_2Cl_2). As expected, the ^{13}C-NMR spectrum also exhibited a low field =CH_2 signal (δ 284.7). The IR spectrum gave an intense ν_{NO} band at 1695 cm^{-1}. A sample was dissolved in C_6D_5Br, and variable temperature ^{1}H-NMR spectra were recorded (400 MHz). The =CH_2 protons still gave distinct signals at 110°C (δ 15.05, 14.10; 15.06, 14.07 at ambient probe temperature). Application of the coalescence formula bounds the $\Delta G^{\ddagger}$ value for methylidene ligand rotation as $>$ 17.5 kcal mol^{-1} (110°C) [16].

Extensive efforts to obtain crystals of **3b**$^+$ BAr_F^- suitable for X-ray analysis were unsuccessful. This included many layered solvent combinations (CH_2Cl_2–hexane, CH_2Cl_2–pentane, $CHCl_2CH_3$–hexane, $CHCl_3$–hexane, CCl_4–hexane), and vapor diffusion ($CHCl_3$–pentane) or slow evaporation (CH_2Cl_2–hexane) conditions. The hexafluoroantimonate salt **3b**$^+$ SbF_6^- was also prepared, and gave similar results. Nonetheless, these failures clearly establish that the crystals of **2b**$^{\bullet+}$ BAr_F^- described above (which could be reproducibly grown from CH_2Cl_2–hexane) are not **3b**$^+$ BAr_F^-. An approximate value for one feature of interest, the Re=CH_2 bond length, can be taken from the crystal structure of the triphenylphosph*ite* complex [(η^5-

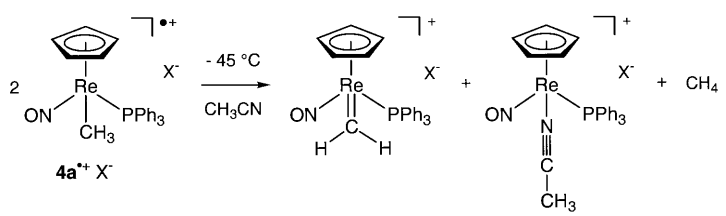

Scheme 2. Thermal disproportionation of the cyclopentadienyl-substituted radical cation **4a**$^{\bullet+}$ X^-.

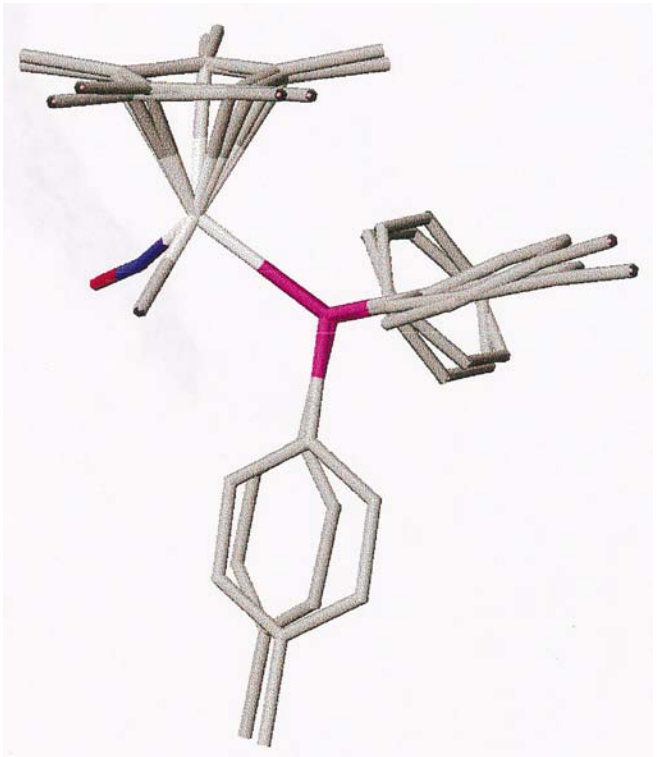

Fig. 3. Superposition of molecular structure of complexes **2b** and **2b**$^{\bullet+}$.

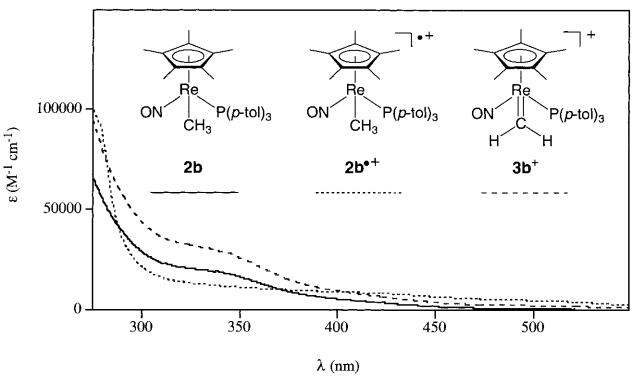

Fig. 4. UV–vis spectra of new complexes.

C_5Me_5)Re(NO)(P(OC_6H_5)$_3$)(=CH_2)]$^+$ PF_6^- (**5**$^+$ PF_6^-; 1.89(2) Å) [13].

In contrast to **3b**$^+$ BAr_F^-, crystals of the 18-valence-electron methyl complex **2b** could (with some effort) be obtained. A crystal structure was determined as outlined in Table 1 and in Section 4. Fig. 2 (top) gives the molecular structure, and Table 2 lists key bond lengths and angles side-by-side with those of **2b**$^{\bullet+}$ BAr_F^-. Fig. 3 gives a superposition of the rhenium moieties of **2b** and **2b**$^{\bullet+}$ BAr_F^-. The small differences are analyzed below.

Finally, the UV–vis spectra of **2b**, **2b**$^{\bullet+}$ BAr_F^-, and **3b**$^+$ BAr_F^- are illustrated in Fig. 4. Although each compound is colored, the spectra show only featureless tails into the visible region. This could have been anticipated for **3b**$^+$ BAr_F^- based upon data for the corresponding vinylidene complex [17]. However, the dirhenium C_4 radical cation **1**$^{\bullet+}$ PF_6^- gives a number of visible and near-IR transitions [7b]. Some of these are diagnostic of its mixed valence redox state. Regardless, none have any counterpart in **2b**$^{\bullet+}$ BAr_F^- (or **2b**).

2.3. Computations

In order to further clarify the structural, electronic, and dynamic properties of the preceding complexes, computational studies were conducted. These utilized two series of model compounds. In the first, abbreviated {Re(PH_3)(CH_3)}, {Re(PH_3)(CH_3)}$^{\bullet+}$ and {Re(PH_3)(=CH_2)}$^+$, the pentamethylcyclopentadienyl and tri(*p*-tolyl)phosphine ligands were replaced by cyclopentadienyl and PH_3. In the second, cyclopentadienyl and PMe_3 ligands were used. Geometries were optimized at the level of density functional theory (B3LYP) with the LANL2DZ basis set and an additional set of polarization functions (LANL2DZp) as introduced by Hay and Wadt [18] and implemented in the GAUSSIAN-98 program [19]. For radical cations, the unrestricted method (UB3LYP) was used. Frequency calculations were carried out at the same level to further characterize the optimized geometries [20].

The computed energies of the model compounds are listed in Table 3. Natural charges and bond orders, calculated with the NBO program [21], are given in Table 4. At the (U)B3LYP/LANL2DZp level, all complexes are energy minima with only real vibrational modes. Selected bond lengths, and bond and torsion angles, are summarized in Figs. 5–7. The data for {Re(PR_3)(CH_3)} (Fig. 5) and {Re(PR_3)(CH_3)}$^{\bullet+}$ (Fig. 6) agree well with the crystal structures, validating the quality of the computational methodology. Hence, the metrical parameters of {Re(PR_3)(=CH_2)}$^+$ (Fig. 7) can be expected to closely match those of **3b**$^+$ BAr_F^-. The methyl and methylidene ligand conformations agree with previous studies at the extended Hückel level [22,23]. Computed ν_{NO} values are also given in Table 4, and are very close to those observed. Frontier molecular orbitals are depicted in Fig. 8.

Rotations about the rhenium–CH_x and rhenium–PH_3 bonds were also investigated computationally. Transition state energies and geometries are summarized in Table 3 and Fig. 9. In the ground state of {Re(PH_3)(CH_3)} (Fig. 5), the methyl carbon–hydrogen bonds are roughly staggered with respect to the other rhenium ligands. However, as observed above, staggered and eclipsed are imprecise conformational descriptors for bonds between formally octahedral and tetrahedral atoms. Thus, we simply note that one hydrogen is anti to the cyclopentadienyl ligand, as reflected by a H_α–C–Re–Cp torsion angle of −179.8°. In the transition state for methyl rotation (Fig. 9), a hydrogen moves into a syn position, as reflected by a

Table 3
Energetic data ((U)B3LYP/LANL2DZp) for model complexes $[(\eta^5\text{-}C_5H_5)Re(NO)(PR_3)(CH_x)]^{n+}$

	E_{tot} (au)	Imaginary frequencies (cm^{-1})	$E_{thermal}$ 298.15 K (kcal mol^{-1})	Entropy 298.15 K (cal mol^{-1})
Ground states				
$\{Re(PH_3)(CH_3)\}$	−450.86336	None	105.5	111.2
$\{Re(PMe_3)(CH_3)\}$	−568.84429			
$\{Re(PH_3)(CH_3)\}^{\bullet+}$	−450.62294	None	106.0	116.5
$\{Re(PMe_3)(CH_3)\}^{\bullet+}$	−568.62316			
$\{Re(PH_3)(=CH_2)\}^{+}$	−450.02338	None	99.0	107.6
$\{Re(PMe_3)(=CH_2)\}^{+}$	−568.02278			
Transition states				
$\{Re(PH_3)(CH_3)\}$ (CH_3 rotation)	−450.86122	154i	105.0	108.2
$\{Re(PH_3)(CH_3)\}$ (PH_3 rotation)	−450.86142	106i	104.9	108.6
$\{Re(PH_3)(=CH_2)\}^{+}$ ($=CH_2$ rotation)	−499.97685	854i	97.6	108.9

$H_{\alpha'}$–C–Re–Cp torsion angle of −1.3°. Apart from these rhenium–CH_3 torsional differences, the ground and transition state structures are remarkably similar. The rhenium–carbon bond does lengthen from 2.186 to 2.193 Å. However, the rhenium–phosphorus and rhenium–Cp bonds, which are not undergoing rotation, similarly elongate.

The phosphine ligand in $\{Re(PH_3)(CH_3)\}$ adopts an opposite ground state conformation (Fig. 5). Now, one hydrogen is nearly syn to the cyclopentadienyl ligand, as indicated by a H3–P–Re–Cp torsion angle of −5.7°. The longer rhenium–phosphorus bond (2.353 Å versus Re–CH_3 2.186 Å) may be a contributing factor. However, when the hydrogens are replaced by larger methyl groups in $\{Re(PMe_3)(CH_3)\}$ (Fig. 5), the conformation changes. One methyl group becomes nearly anti to the cyclopentadienyl ligand, as reflected by a C1–P–Re–Cp torsion angle of 187.1°. Regardless, the transition state for phosphine rotation in $\{Re(PH_3)(CH_3)\}$ features a hydrogen anti to the cyclopentadienyl ligand (Fig. 9; H2–P–Re–Cp torsion angle −187.5°), and only slight changes in bond distances. Importantly, the transition states for methyl and phosphine rotation exhibit only a single imaginary frequency (Table 3). Hence, they can confidently be assigned as real transition states.

Table 4
Computed natural charges, bond orders, and ν_{NO} vibrational modes (cm^{-1}) for the $[(\eta^5\text{-}C_5H_5)Re(NO)(PH_3)(CH_x)]^{n+}$ ground states

	$\{Re(PH_3)(CH_3)\}$	$\{Re(PH_3)(CH_3)\}^{\bullet+}$	$\{Re(PH_3)(=CH_2\}^{+}$
Re	0.222	0.574	0.336
CH_x	−0.276	−0.155	0.036
PH_3	0.404	0.482	0.539
NO	−0.166	0.003	0.021
$\eta^5\text{-}C_5H_5$	−0.182	0.096	0.068
Re–C	0.709	0.903	1.428
Re–N	1.793	1.489	1.491
Re–P	0.609	0.576	0.651
P–H1	0.942	0.921	0.924
P–H2	0.958	0.918	0.929
P–H3	0.979	0.942	0.933
ν_{NO} [a]	1613 (1603)	1714 (1714)	1714 (1695)

[a] Experimental values for **2b**, $\mathbf{2b}^{\bullet+}$ BAr_F^- and $\mathbf{3b}^{+}$ BAr_F^- are given in parenthesis.

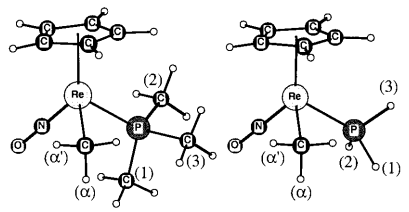

	$\{Re(PMe_3)(CH_3)\}$	$\{Re(PH_3)(CH_3)\}$	X-Ray, **2b**
Re-C	2.191	2.186	2.123
Re-P	2.384	2.353	2.359
Re-N	1.759	1.766	1.787
Re-Cp	1.991	1.984	1.970
N-O	1.201	1.196	1.175
P-R1	1.859	1.438	1.825
P-R2	1.865	1.427	1.829
P-R3	1.865	1.428	1.839
C-Re-P	85.9	85.9	88.1
C-Re-N	94.8	94.9	97.9
P-Re-N	91.8	92.7	92.7
H_α-C-Re-P	-53.4	-55.4	
H_α-C-Re-N	38.1	37.0	
H_α-C-Re-Cp	-178.1	-179.8	
$H_{\alpha'}$-C-Re-Cp	63.0	61.0	
C1-P-Re-C	72.1		36.0
C1-P-Re-N	-22.6		-61.8
C1-P-Re-Cp	187.1		161.1
H3-P-Re-C		-120.8	
H3-P-Re-N		144.4	
H3-P-Re-Cp		-5.7	
H2-P-Re-Cp		-123.6	

Fig. 5. Structural parameters (Å, °) for $[(\eta^5\text{-}C_5H_5)Re(NO)(PR_3)(Me)]$ at the B3LYP/LANL2DZp level.

Activation parameters can be derived from Table 3. The $\Delta H^{\ddagger}$ values for methyl and phosphine rotation in $\{Re(PH_3)(CH_3)\}$ are 0.9 and 0.6 kcal mol^{-1}, respectively (298.15 K). The corresponding $\Delta S^{\ddagger}$ values are -3.0 and -2.6 cal mol^{-1}, and $\Delta G^{\ddagger}$ values are 1.8 and 1.4 kcal mol^{-1}. There is ample precedent for rotational barriers of this magnitude in transition metal methyl complexes [24], although much higher barriers are possible with more congested metal fragments, and alkyl or phosphine ligands [25]. Attempts to locate the transition state for methyl rotation in the radical cation $\{Re(PH_3)(CH_3)\}^{\bullet+}$ failed. This indicates that the energy barrier cannot be higher than that of the neutral complex.

The geometry of the transition state for methylidene rotation in $\{Re(PH_3)(=CH_2)\}^{+}$ matches that calculated earlier by extended Hückel theory [22a]. As shown in Fig. 9, the plane of the ligand rotates ca. 90°, as reflected by the new H_{α}–C–Re–P and $H_{\alpha'}$–C–Re–N torsion angles ($-82.6°$ versus $-176.5°$; 9.3° versus $-78.8°$). Unlike methyl rotation in $\{Re(PH_3)(CH_3)\}$, the conformation of the phosphine significantly changes. The $\Delta H^{\ddagger}$ and $\Delta S^{\ddagger}$ values computed from Table 3 are 27.9 kcal mol^{-1} and 1.3 cal mol^{-1} (298.15 K). These give a $\Delta G^{\ddagger}_{383\ K}$ value of 27.4 kcal mol^{-1}, consistent with that bounded by NMR for the much more congested species **3b**$^{+}$ BAr_F^- (>17.5 kcal mol^{-1}), as well as triphenylphosphine and triphenylphosphite analogs **3a**$^{+}$ PF_6^- and **5**$^{+}$ PF_6^- (>19 kcal mol^{-1}) [13]. Some cyclopentadienyl analogs $[(\eta^5\text{-}C_5H_5)Re(NO)(PPh_3)(=CHR)]^{+}$ X^- can be generated as non-equilibrium mixtures of geometric isomers, and rate studies give $\Delta G^{\ddagger}$ values of ca. 20 kcal mol^{-1} [22a,26].

3. Discussion

To our knowledge, **2b** and **2b**$^{\bullet+}$ BAr_F^- represent only the second structurally characterized pair of 18- and 17-valence-electron complexes of the 'piano stool' formula $(\eta^5\text{-}C_5R_5)M(L)(L')(L'')$. Crystal structures of the chromium complexes $(\eta^5\text{-}C_5H_5)Cr(NO)(P(OMe)_3)_2$ and $[(\eta^5\text{-}C_5H_5)Cr(NO)(P(OMe)_3)_2]^{\bullet+}$ PF_6^- were previously reported by Legzdins, Einstein and coworkers [4f]. The closely related 17/18-electron species $(\eta^5\text{-}C_5Me_5)Fe(dppe)(CH_2OMe)]^{\bullet+}$ PF_6^- and $(\eta^5\text{-}C_5Me_5)Fe(dppe)(C{\equiv}CH)$ [4a,27], and $(\eta^5\text{-}C_5H_5)Cr(NO)(PPh_3)(CH_2SiMe_3)$ and $(\eta^5\text{-}C_5H_5)Fe(CO)(PPh_3)(CH_2SiMe_3)$ [4e,28] also deserve mention. However, more exact comparisons can be made with otherwise identical compounds, such as **2b** and **2b**$^{\bullet+}$ BAr_F^-.

In this context, a landmark study of Orpen and Connelly merits emphasis [29]. These authors compared nine high-quality crystal structures of homologous neutral 18- and cationic 17-valence-electron phosphine and phosphite complexes (although none of the 'piano stool' variety). They found that the metal–phosphorus ($M–PX_3$) bonds lengthened upon oxidation. However, the P–X bond distances decreased. This was interpreted as evidence for the participation of P–X σ*-orbitals in phosphine ligand backbonding. A stronger interaction would be expected in the 18-electron systems, leading to longer P–X bonds. This is readily visualized from the HOMO of $\{Re(PH_3)(CH_3)\}$ shown in Fig. 8(B). There is a large degree of rhenium d-orbital 'lone pair' character, resulting in slight P–H σ* character for the appropriately aligned bond. The singly-occupied HOMO (SOMO) of radical cation $\{Re(PR_3)(CH_3)\}^{\bullet+}$ has a much different electron distribution.

The first question is then 'how different are the crystal structures of **2b** and **2b**$^{\bullet+}$ BAr_F^-?' The overlay in Fig. 3 shows that the rhenium moieties exhibit very similar structures. The eight-atom $Re(NO)(CH_3)P(C_{ipso})_3$ segments are virtually superimposable. The greatest difference is in one P–C_{ipso} conformation, a slight effect that could easily be due to packing forces. However, the esd values associated with the crystallographic data are only of average quality

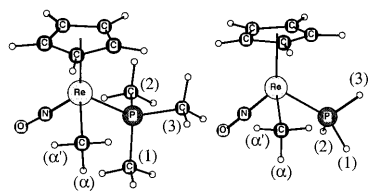

	$\{Re(PMe_3)(CH_3)\}^{\bullet+}$	$\{Re(PH_3)(CH_3)\}^{\bullet+}$	X-Ray, **2b**$^{\bullet+}$ BAr_F^-
Re-C	2.137	2.143	2.120
Re-P	2.469	2.474	2.455
Re-N	1.772	1.779	1.813
Re-Cp	2.025	2.008	1.985
N-O	1.177	1.171	1.027
P-R1	1.850	1.422	1.827
P-R2	1.851	1.420	1.811
P-R3	1.850	1.420	1.805
C-Re-P	94.9	92.4	89.8
C-Re-N	93.3	92.4	99.7
P-Re-N	91.2	94.0	91.8
H_{α}-C-Re-P	-47.1	-49.1	
H_{α}-C-Re-N	44.5	44.9	
H_{α}-C-Re-Cp	-177.4	-179.4	
$H_{\alpha'}$-C-Re-Cp	64.1	62.3	
C1-P-Re-C	41.6		44.2
C1-P-Re-N	-51.8		-55.5
C1-P-Re-Cp	164.8		170.6
H3-P-Re-C		-105.6	
H3-P-Re-N		161.8	
H3-P-Re-Cp		15.1	

Fig. 6. Structural parameters (Å, °) for $[(\eta^5\text{-}C_5H_5)Re(NO)(PR_3)(Me)]^{\bullet+}$ at the UB3LYP/LANL2DZp level.

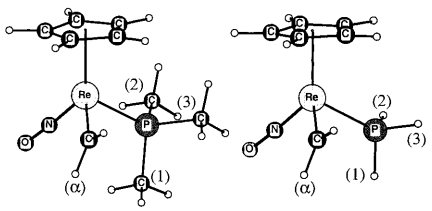

{Re(PMe$_3$)(=CH$_2$)}$^+$ {Re(PH$_3$)(=CH$_2$)}$^+$

Re-C	1.918	1.923
Re-P	2.448	2.430
Re-N	1.772	1.780
Re-Cp	2.034	2.023
N-O	1.178	1.172
P-R1	1.848	1.418
P-R2	1.851	1.421
P-R3	1.849	1.418
C-Re-P	93.0	92.2
C-Re-N	95.8	95.6
P-Re-N	89.9	91.6
H_α-C-Re-P	-82.2	-82.6
H_α-C-Re-N	7.9	9.3
H_α-C-Re-Cp	152.1	152.2
R1-P-Re-C	51.6	51.9
R1-P-Re-N	-44.2	-43.8
R1-P-Re-Cp	176.9	177.0

Fig. 7. Structural parameters (Å, °) for [(η^5-C_5H_5)Re(NO)(PR_3)(=CH_2)]$^+$ at the B3LYP/LANL2DZp level.

(Table 2), and it is often difficult to be certain that one bond length or angle is greater than another. In these cases, the computational data (Figs. 5 and 6) provide reliable answers.

Regardless, the crystallographic distances between the heavy rhenium and phosphorus atoms in **2b** and **2b**$^{\bullet+}$ BAr_F^- are very accurately determined. The increase from 2.359(2) to 2.455(3) Å is typical of those found by Orpen and Connelly [29]. The computational data for {Re(PR_3)(CH_3)} and {Re(PR_3)(CH_3)}$^{\bullet+}$ show nearly identical increases (R = H, 2.353–2.474 Å; R = Me, 2.384–2.469 Å), as well as an accompanying decrease in bond order (Table 4). The rhenium–nitrogen bonds show a less pronounced lengthening (R = H, 1.766 versus 1.779 Å; R = Me, 1.759 versus 1.772 Å), but a more pronounced bond order decrease. The rhenium–nitrogen bond lengths of **2b** and **2b**$^{\bullet+}$ BAr_F^- have esd values too large to allow meaningful comparisons (1.787(9) versus 1.813(12) Å).

It is similarly difficult to contrast the phosphorus–carbon bond lengths in **2b** and **2b**$^{\bullet+}$ BAr_F^- (1.825(8) versus 1.827(11) Å; 1.829(9) versus 1.811(11) Å; 1.839(9) versus 1.805(12) Å). Two of the three appear to be shorter. However, the computational data for {Re(PR_3)(CH_3)}$^{\bullet+}$ show unambiguous and relatively uniform P–R bond contractions averaging 0.010 Å and 0.013 Å (R = H, Me). These are somewhat smaller than the decreases found by Orpen and Connelly [29]. The small anisotropy in the reductions has prompted us to consider other contributions. For example, in work in progress, we compute substantial P–C bond contractions upon protonation of PPh_3 to $[HPPh_3]^+$ (1.854 versus 1.801 Å) [30]. The examples of Orpen and Connelly similarly feature neutral and cationic homologs. Table 4 shows that positive charge on phosphorus increases upon going from {Re(PR_3)(CH_3)} to {Re(PR_3)(CH_3)}$^{\bullet+}$.

The complexes of Legzdins [4f], (η^5-C_5H_5)Cr(NO)($P(OMe)_3$)$_2$ and [(η^5-C_5H_5)Cr(NO)($P(OMe)_3$)$_2$]$^{\bullet+}$ PF_6^-, exhibit similar relationships. The chromium–phosphorus bonds lengthen from 2.227(2)–2.240(2) Å (two independent molecules in unit cell) to 2.343(2)–2.346(3) Å, which the authors attributed to a diminution in back-bonding. The phosphorus–oxygen bond lengths were not interpreted, perhaps due to disorder of the phosphite ligand in both species. However, the refined data indicate a contraction from 1.580(4)–1.623(6) Å (average and standard deviation for twelve bonds: 1.601(3) ± 0.0038 Å) to 1.562(5)–1.578(4) Å (average and standard deviation for six bonds: 1.568(8) ± 0.0026 Å).

The rhenium–methyl bond lengths in **2b** and **2b**$^{\bullet+}$ BAr_F^- can also be analyzed. The crystallographic distances are essentially identical (2.123(11) versus 2.120(12) Å), a trend we are attempting to further support with analogs of **2b**. For example, the cyclopentadienyl benzyl complex (*R*)-(η^5-C_5H_5)Re(NO)(PPh_3)($CH_2C_6H_5$) exhibits a longer rhenium–carbon bond (2.203(8) Å) [31], as does a similar secondary alkyl complex [32]. The computational data for {Re(PR_3)(CH_3)} and {Re(PR_3)(CH_3)}$^{\bullet+}$ show distinct contractions (R = H, 2.186 versus 2.143 Å; R = Me, 2.191 versus 2.137 Å) and increased bond order (Table 4), opposite to the trends with the phosphine and nitrosyl ligands. This can be rationalized from several perspectives. First, methyl is the poorest π accepting ligand, so the π bond order should be least affected by oxidation. Second, the carbon–hydrogen bonding electron pairs are possible sources of repulsive interactions with filled metal orbitals in 18-valence-electron systems [33]. For example, an antibonding interaction is apparent in the HOMO of {Re(PH_3)(CH_3)} shown in Fig. 8(B). Third, the carbon–hydrogen bonding electron pairs can supply hyperconjugative stabilization after oxidation.

Methylidene ligands are strong π acceptors [34], and numerous complexes are known with high degrees of metal-double bond character [14]. Accordingly, the rhenium–carbon bond lengths computed for {Re(PR_3)(=CH_2)}$^+$ are much shorter than those in methyl complexes {Re(PR_3)(CH_3)} (R = H, 1.923 ver-

sus 2.186 Å; R = Me, 1.918 versus 2.191 Å), and in good agreement with the triphenylphosph*ite* complex $\mathbf{5}^{+}$ PF_6^- (1.89(2) Å) [13]. As expected, the rhenium–carbon bond order is much higher (Table 4). In the ground state conformation, the methylidene ligand competes with the phosphine for the d-orbital HOMO of the rhenium fragment (Fig. 8(A)). Thus, the rhenium–phosphorus bonds are longer than those in $\{Re(PR_3)(CH_3)\}$ (R = H, 2.430 versus 2.353 Å; R = Me, 2.448 versus 2.384 Å), although still slightly shorter than in radical cations $\{Re(PR_3)(CH_3)\}^{\bullet +}$ (R = H, 2.474 Å; R = Me, 2.469 Å). Also, the P–R distances are shorter than those in the neutral complexes, and close to those of the radical cations. However, the rhenium–phosphorus bond order is higher in $\{Re(PH_3)(=CH_2)\}^{+}$ than $\{Re(PR_3)(CH_3)\}$ (Table 4), suggesting an underlying σ-orbital effect.

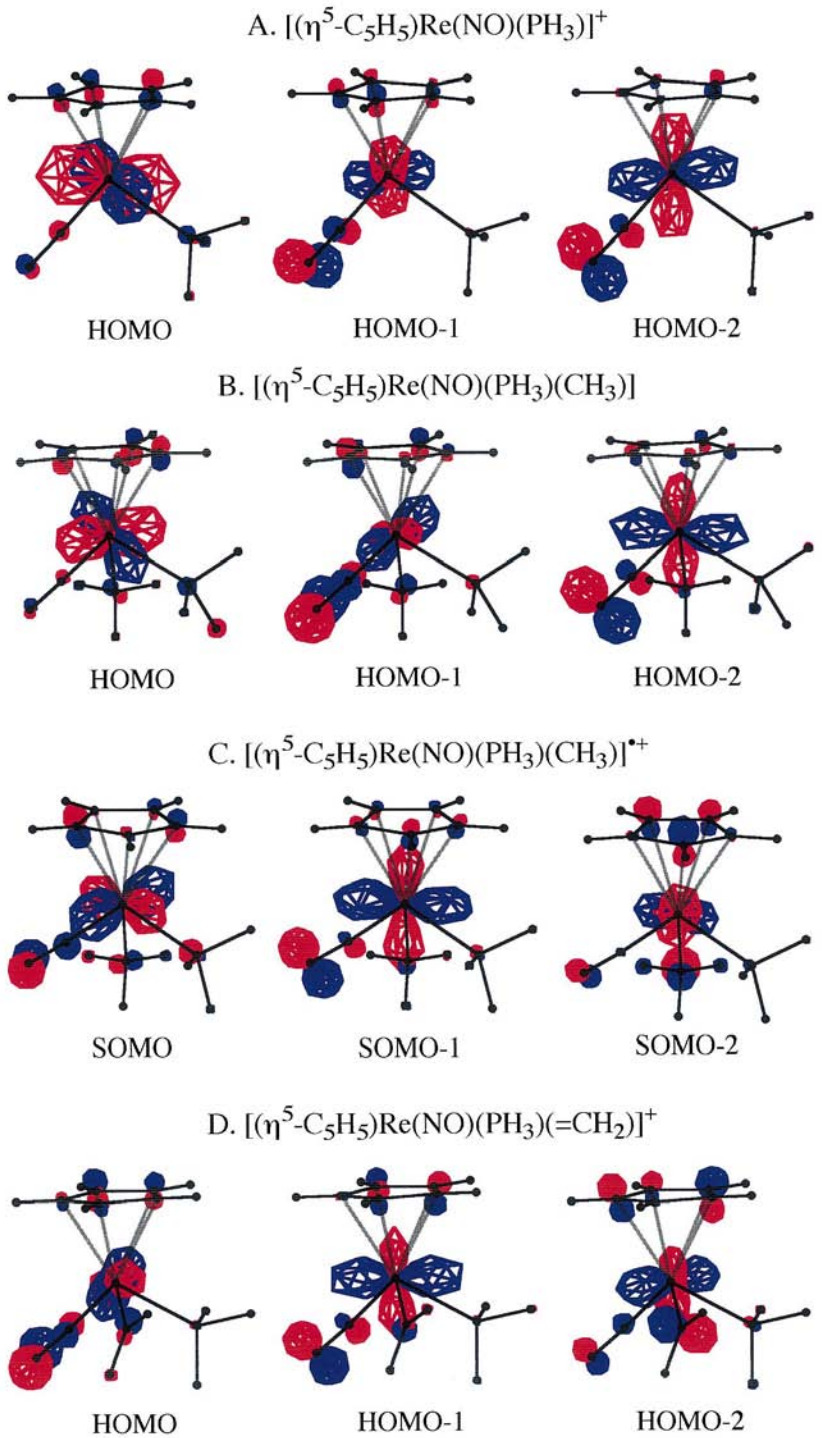

Fig. 8. Frontier molecular orbitals of model complexes.

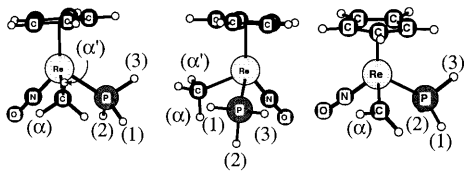

Transition state	{Re(PH$_3$)(CH$_3$)}, CH$_3$ rotation	{Re(PH$_3$)(CH$_3$)}, PH$_3$ rotation	{Re(PH$_3$)(=CH$_2$)}$^+$, =CH$_2$ rotation
Re-C	2.193	2.193	1.983
Re-P	2.360	2.364	2.399
Re-N	1.763	1.764	1.826
Re-Cp	1.990	1.983	1.985
N-O	1.195	1.196	1.164
P-H1	1.437	1.428	1.429
P-H2	1.428	1.430	1.421
P-H3	1.427	1.430	1.421
C-Re-P	86.8	83.8	88.2
C-Re-N	94.1	95.0	90.2
P-Re-N	92.3	92.4	97.7
H$_\alpha$-C-Re-P	-119.1	-58.5	-176.5
H$_\alpha$-C-Re-N	-26.9	33.4	-78.8
H$_\alpha$-C-Re-Cp	116.1	176.5	58.7
H$_{\alpha'}$-C-Re-Cp	-1.3	57.9	
H3-P-Re-C	-123.0	-180.6	-121.8
H3-P-Re-N	143.0	84.7	148.2
H3-P-Re-Cp	-5.4	-66.7	4.7
H2-P-Re-Cp	-123.3	-187.5	-113.5

Fig. 9. Structural parameters (Å, °) of the transition states for ligand rotation at the B3LYP/LANL2DZp level.

The transition state for methylene rotation in {Re(PH$_3$)(=CH$_2$)}$^+$ (Fig. 9) features a longer rhenium–carbon bond than the ground state (1.983 versus 1.923 Å). However, the bond remains much shorter than in the ground states of methyl complexes {Re(PH$_3$)(CH$_3$)} and {Re(PH$_3$)(CH$_3$)}$^{\bullet+}$ (2.186 and 2.143 Å). This indicates a reduced but still significant π bond order. In the transition state conformation, the methylene ligand competes with the nitrosyl for another of the d donor orbitals on rhenium. Accordingly, the rhenium–nitrogen bond is much longer than in the ground state (1.826 versus 1.780 Å). Also, the rhenium–phosphorus bond contracts (2.399 versus 2.430 Å), and one of the three phosphorus–hydrogen bonds lengthens (average: 1.424 versus 1.419 Å). The Orpen–Connelly model predicts longer phosphorus–hydrogen bonds.

The preceding calculations also illustrate a number of conformational features and subtleties that have been analyzed in previous publications in this series [22,23,35], and in related work by others [28]. However, the purpose of this discussion is to emphasize the new insights afforded by the radical cations **2b**$^{\bullet+}$ BAr$_F^-$ and {Re(PR$_3$)(CH$_3$)}$^{\bullet+}$. These represent both experimental and computational breakthroughs, as earlier calculations of related species failed to give SCF convergence [7b]. Similarly, the frontier orbitals in Fig. 9 resemble those obtained with lower levels of theory [22,23d,36], and are not analyzed further. However, we are conducting an extensive computational study of dirhenium C_x complexes of the formula [(η^5-C$_5$R$_5$)Re(NO)(PR$_3$)-(C$_x$)(R$_3$P)(ON)Re(η^5-C$_5$R$_5$)]$^{n+}$, and the preceding energies, geometries, and orbitals constitute important benchmarks for this much more involved undertaking [37].

Some purely experimental aspects of this study merit further analysis. First, we are somewhat surprised by the apparent lack of reactivity of **2b**$^{\bullet+}$ BAr$_F^-$ towards phosphine substitution. There are many well documented associative substitutions of 17-valence-electron 'piano stool' complexes, involving both transient [38] and isolated [4e,39] species. However, marked steric effects have been observed [4e]. Except for (η^5-C$_5$H$_5$)W(CO)$_3^{\bullet}$ [38e] and the chain process in the previous paper [6], examples involving third-row metals appear to be rare. Nonetheless, other interesting reactivity modes can be anticipated. For example, in collaborative studies with Parker, we showed that reactions of cyclopentadienyl alkyl complexes (η^5-C$_5$H$_5$)Re(NO)-(PPh$_3$)(CHRCHR′) and trityl cations proceed by initial electron transfer to give rhenium radical cations and trityl radicals [40]. Then hydrogen atom transfer occurs. Hence, **2b**$^{\bullet+}$ BAr$_F^-$ is likely to be an effective hydrogen atom donor, and is a probable intermediate in the synthesis of **3b**$^+$ BAr$_F^-$ in Scheme 1.

Second, the original motivation of this study was to obtain longer chain homologs of the C_4 dirhenium radical cation **1**$^{\bullet+}$ PF$_6^-$ and dication **1**$^{2+}$ 2PF$_6^-$ with enhanced stabilities [6]. The above data show that an *anion effect* can be added to the *phosphine effect* described in the preceding paper [6]. Such anion effects have precedent [9], but are generally not amenable to single-parameter explanations. Nonetheless, it is instructive to note that the formula weight and unit cell volume of **2b**$^{\bullet+}$ BAr$_F^-$ are factors of 2.28 and 2.22 greater than those of **2b** (both crystallize as monoclinic systems with $Z = 4$). In conclusion, this paper describes an important refinement in our 'first generation' approach to the C_x target complexes described above. The next strategic step in this ultimately successful quest will be the subject of a future communication [41].

4. Experimental

4.1. General data

Many general procedures were identical with those in the previous paper [6], but most work was conducted at a new location. Thus, the following instruments differed: NMR, Jeol JMN-400CX spectrometer (stan-

dards: ^{1}H, residual internal C_6D_5H (δ 7.16), $CDHCl_2$ (δ 5.32), CD_2HCN (δ 1.94); ^{13}C, internal CD_2Cl_2 (δ 54.00); ^{31}P, external 85% H_3PO_4 (δ 0.00)); IR, Bruker IFS 25 or React-IR™ 1000 Reaction Analysis System; UV–vis, Shimadzu UV-3102 PC; ESR, Bruker ESP-3000E (ER 4116 DM dual mode X-band cavity, Oxford Instruments ESR-900 helium flow cryostat; spectra at modulation amplitude 12.6 G and sweep rate 100 G s^{-1}), mass spectrometry, Micromass Zabspec; cyclic voltammetry, BAS model CV-50W; microanalyses, Carlo Erba model EA1110 (all measurements in-house). All manipulations were carried out under N_2 that had been dried with KOH and $CaCl_2$. Hexane (> 95% GC grade, Fluka) was distillated from sodium, CH_2Cl_2 (99.9% HPLC grade, Sigma-Aldrich) from CaH_2, and benzene from Na–benzophenone. CD_3CN was refluxed over CaH_2, vacuum-transferred, and freeze-pump-thaw degassed. Other materials, $(\eta^5\text{-}C_5H_5)_2Fe$ (Fluka), and $(\eta^5\text{-}C_5H_5)_2Co^{\bullet}$ (Acros), were used as received.

4.2. $(\eta^5\text{-}C_5H_5)_2Fe^{\bullet+}$ BAr^-_F [9b]

A Schlenk flask was charged with $(\eta^5\text{-}C_5H_5)_2Fe$ (0.150 g, 0.806 mmol), acetone (1.2 ml), and water (4 ml). The suspension was stirred, and solid $FeCl_3\cdot 6H_2O$ (0.360 g, 1.331 mmol) was added. After 15 min, the dark blue solution was filtered. Then Na^+ BAr^-_F (0.710 g, 0.801 mmol) [15,42] was added to the filtrate. After 20 min, a dark precipitate was removed by filtration, washed with water (2 × 2 ml) and hexane (2 × 2 ml), and dried by oil pump vacuum (3 h). The residue was extracted with CH_2Cl_2 (10 ml). The mixture was filtered, and hexane (5 ml) was added to the filtrate. The sample was concentrated under vacuum. The dark blue solid was collected by filtration and washed with hexane (2 × 5 ml) to give $(\eta^5\text{-}C_5H_5)_2Fe^{\bullet+}$ BAr^-_F (0.676 g, 0.644 mmol; 80%). $C_{42}H_{22}BF_{24}Fe$: Anal. Found: C, 47.70; H, 2.07. Calc. C, 48.08; H, 2.11%.

4.3. $[(\eta^5\text{-}C_5Me_5)Re(NO)(P(4\text{-}C_6H_4CH_3)_3)(CH_3)]^{\bullet+}$ BAr^-_F (**2b**$^{\bullet+}$ BAr^-_F)

A Schlenk flask was charged with $(\eta^5\text{-}C_5Me_5)Re(NO)(P(4\text{-}C_6H_4CH_3)_3)(CH_3)$ (**2b** [6]; 0.030 g, 0.044 mmol) and CH_2Cl_2 (3 ml). Then solid $(\eta^5\text{-}C_5H_5)_2Fe^{\bullet+}$ BAr^-_F (0.047 g, 0.044 mmol) was added with stirring. After 10 min, solvent was removed from the orange–brown solution by oil pump vacuum. The residue was washed with hexane (2 × 3 ml) and dissolved in CH_2Cl_2 (1 ml). The solution was added to rapidly stirred cold hexane (30 ml, −78°C, acetone–CO_2). After 10 min, solvent was removed by cannula. The tan powder was dried by oil pump vacuum as the cold bath was allowed to warm to room temperature (this period includes 1 h at room temperature) to give **2b**$^{\bullet+}$ BAr^-_F (0.054 g, 0.035 mmol; 80%), m.p. (dec) 140–148°C. IR (CH_2Cl_2) $\nu_{NO} = 1714$ cm^{-1} s. $C_{64}H_{51}BF_{24}NOPRe$: Anal. Found: C, 49.56; H, 3.14; N, 0.95. Calc. C, 50.10; H, 3.35; N, 0.91%.

4.4. Reduction of **2b**$^{\bullet+}$ BAr^-_F

A Schlenk flask was charged with **2b**$^{\bullet+}$ BAr^-_F (0.045 g, 0.029 mmol) and CH_2Cl_2 (2 ml). Then solid $(\eta^5\text{-}C_5H_5)_2Co^{\bullet}$ (0.005 g, 0.029 mmol) was added with stirring. After 10 min, solvent was removed by oil pump vacuum. The residue was extracted with benzene (3 × 10 ml). The solution was filtered through a silica gel pad. The filtrate was taken to dryness by oil pump vacuum. The residue was recrystallized from CH_2Cl_2–hexane to give **2b** as an orange powder (0.017 g, 0.026 mmol, 90%). ^{1}H-NMR (C_6D_6, 400 MHz): $\delta = 7.59$ (pseudo t, $J_{HP} = J_{HH} = 8.6$, 3*o*-C_6H_4), 6.93 (d, $J_{HH} = 8.2$ Hz, 3*m*-C_6H_4), 1.99 (s, 3ArCH_3), 1.62 (s, $C_5(CH_3)_5$), 1.37 (br s, ReCH_3).

4.5. $[(\eta^5\text{-}C_5Me_5)Re(NO)(P(4\text{-}C_6H_4CH_3)_3)(=CH_2)]^+$ BAr^-_F (**3b**$^+$ BAr^-_F)

A Schlenk flask was charged with **2b** (0.061 g, 0.091 mmol) and CH_2Cl_2 (5 ml) and cooled to −78°C (acetone–CO_2). Then Ph_3C^+ BAr^-_F (0.101 g, 0.091 mmol) [15] was added against a N_2 flow with stirring. After 3.5 h at −78°C, hexane (10 ml) was added. The sample was concentrated under vacuum at 0°C, giving a precipitate. Then more hexane (15 ml) was added. After 10 min, the yellow precipitate was collected by filtration, washed with hexane (2 × 5 ml), and dried by oil pump vacuum (1 h) to give **3b**$^+$ BAr^-_F (0.112 g, 0.073 mmol; 80%), m.p. (dec.) 160–170°C. IR (solid film) $\nu_{NO} =$ 1695 cm^{-1} s. ^{1}H-NMR (CD_2Cl_2, 400 MHz) $\delta = 15.17$ and 14.22 (2dd, $J_{HH'} = 6$ Hz, $J_{HP} = 1.6$ Hz, =C*HH*′), 7.72 (br s, 4*o*-BC_6H_3), 7.55 (br s, 4*p*-BC_6H_3), 7.35–7.32, 7.22–7.17 (m, 3*o*,*m*-PC_6H_4), 2.41 (s, 3ArCH_3), 1.88 (s, $C_5(CH_3)_5$). $^{13}C\{^1H\}$ (100.4 MHz) $\delta = 284.7$ (br s, =CH_2), 162.5 (q, $J_{CB} = 49.8$ Hz, *i*-BC_6H_3), 144.3 (s, *p*-PC_6H_4), 135.5 (br s, *o*-BC_6H_3), 133.4 (d, $J_{CP} = 12$ Hz, *o*-PC_6H_4), 130.8 (d, $J_{CP} = 10$ Hz, *m*-PC_6H_4), 130.5–129.1 (m, *i*-PC_6H_4, *m*-BC_6H_3), 125.2 (q, $J_{CF} = 270$ Hz, CF_3), 118.1 (br s, *p*-BC_6H_3), 111.3 (s, $C_5(CH_3)_5$), 21.6 (s, ArCH_3), 10.3 (s, $C_5(CH_3)_5$). $^{31}P\{^1H\}$ (161.7 MHz) $\delta =$ 22.8 (s). MS (positive FAB, 3-NBA–CH_2Cl_2): 670 (**3b**$^+$, 40%), 656 (**3b**-CH_2^+, 100%). $C_{64}H_{50}BF_{24}NOPRe$: Anal. Found: C, 50.44; H, 3.36; N, 0.89. Calc. C, 50.14; H, 3.29; N, 0.91%.

4.6. Crystallography

Slow evaporation of a saturated CH_2Cl_2–hexane solution of **2b** afforded orange prisms. A CH_2Cl_2 solution of **2b**$^{\bullet+}$ BAr^-_F was layered with hexane in a dry box. Dark brown prisms formed. Data were collected as

outlined in Table 1 using a Nonius MACH3 diffractometer. Cell parameters were obtained from 15 reflections with $5.0 < 2\theta < 50.0°$. The space groups were determined from systematic absences ($h01$, $1 = 2n$; $0k0$, $k = 2n$) and subsequent least-squares refinement. Empirical absorption corrections were applied (Ψ-scans). The structures were solved by direct methods using SHELXS-86. Then SHELXS-93 [43] was used to refine 325 (**2b**) or 838 (**2b**$^{\bullet+}$ BAr_F^-) parameters with all data by full-matrix least-squares on F^2. Non-hydrogen atoms were refined anisotropically. The hydrogen atoms were fixed in idealized positions using a riding model.

5. Supplementary material

All data (excluding structure factors) have been deposited with the Cambridge Crystallographic Data Centre, CCDC nos. 140674 (**2b**) and 140675 (**2b**$^{\bullet+}$ BAr_F^-). Copies of this information may be obtained free of charge from The Director, CCDC, 12 Union Road, Cambridge CB2 1EZ, UK (Fax: +44-1223-336033; e-mail: deposit@ccdc.cam.ac.uk or www: http://www.ccdc.cam.ac.uk).

Acknowledgements

We thank the Deutsche Forschungsgemeinschaft (DFG, GL 300/2-1) for financial support, and Professor Dr Ulrich Zenneck and Matthias Zeller of the Institut für Anorganische Chemie for assistance with the ESR spectra.

References

[1] D. Astruc, Electron Transfer and Radical Processes in Transition-Metal Chemistry, VCH, New York, 1995.
[2] M.C. Baird, Chem. Rev. 88 (1988) 1217.
[3] A recent leading reference: K. Costuas, J.-Y. Saillard, Organometallics 18 (1999) 2505.
[4] Structurally characterized 17-valence-electron (η^5-C_5R_5)M(L)(L′)(L″) systems: (a) [(η^5-C_5Me_5)Fe($Ph_2PCH_2CH_2PPh_2$)(CH_2OMe)]$^{\bullet+}$ PF_6^-: C. Roger, L. Toupet, C. Lapinte, J. Chem. Soc. Chem. Commun. (1988) 713. (b) (η^5-C_5H_5)Cr(CO)$_2$(PR_3)$^{\bullet}$ (R = Ph, Me): S. Fortier, M.C. Baird, K.F. Preston, J.R. Morton, T. Ziegler, T.J. Jaeger, W.C. Watkins, J.H. MacNeil, K.A. Watson, K. Hensel, Y. Le Page, J.P. Charland, A.J. Williams, J. Am. Chem. Soc. 113 (1991) 542. (c) [(η^5-C_5Me_5)Fe($Ph_2PCH_2CH_2PPh_2$)(D)]$^{\bullet+}$ PF_6^-: P. Hamon, L. Loupet, J.-R. Hamon, C. Lapinte, Organometallics 11 (1992) 1429. (d) (η^5-C_5Ph_5)Cr(CO)$_3^{\bullet}$: R.J. Hoobler, M.A. Hutton, M.M. Dillard, M.P. Castellani, A.L. Rheingold, A.L. Rieger, P.H. Rieger, T.C. Richards, W.E. Geiger, Organometallics 12 (1993) 116. (e) (η^5-C_5H_5)Cr(NO)(PPh_3)(CH_2SiMe_3)$^{\bullet}$: P. Legzdins, M.J. Shaw, R.J. Batchelor, F.W.B. Einstein, Organometallics 14 (1995) 4721. (f) [(η^5-C_5H_5)Cr(NO)(P(OMe)$_3$)$_2$]$^{\bullet+}$ PF_6^-: P. Legzdins, W.S. McNeil, R.J. Batchelor, F.W.B. Einstein, J. Am. Chem. Soc. 117 (1995) 10521.
[5] Other types of structurally characterized 17-valence-electron rhenium complexes: (a) [(η^5-C_5H_5)Re($NCCH_3$)(PPh_3)$_2$(H)]$^{\bullet+}$ PF_6^-: M.R. Detty, W.D. Jones, J. Am. Chem. Soc. 109 (1987) 5666. (b) Re(CO)$_3$(P(c-C_6H_{11})$_3$)$_2^{\bullet}$: L.S. Crocker, D.M. Heinekey, G.K. Schulte, J. Am. Chem. Soc. 111 (1989) 405. (c) There is also an extensive literature involving paramagnetic rhenium complexes in which the odd electron is ligand-centered: A. Klein, C. Vogler, W. Kaim, Organometallics 15 (1996) 236.
[6] W.E. Meyer, A.J. Amoroso, M. Jaeger, J. Le Bras, W.-T. Wong, J.A. Gladysz, J. Organomet. Chem. 616 (2000) 44.
[7] Full papers with extensive literature background: (a) W. Weng, T. Bartik, M. Brady, B. Bartik, J.A. Ramsden, A.M. Arif, J.A. Gladysz, J. Am. Chem. Soc. 117 (1995) 11922. (b) M. Brady, W. Weng, Y. Zhou, J.W. Seyler, A.J. Amoroso, A.M. Arif, M. Böhme, G. Frenking, J.A. Gladysz, J. Am. Chem. Soc. 119 (1997) 775. (c) S.B. Falloon, S. Szafert, A.M. Arif, J.A. Gladysz, Chem. Eur. J. 4 (1998) 1033. (d) T. Bartik, W. Weng, J.A. Ramsden, S. Szafert, S.B. Falloon, A.M. Arif, J.A. Gladysz, J. Am. Chem. Soc. 120 (1998) 11071. (e) R. Dembinski, T. Bartik, B. Bartik, M. Jaeger, J.A. Gladysz, J. Am. Chem. Soc. 122 (2000) 810.
[8] $BAr_F^- = B(3,5\text{-}C_6H_3(CF_3)_2)_4^-$.
[9] (a) J. Huhmann-Vincent, B.L. Scott, G.J. Kubas, Inorg. Chem. 38 (1999) 115 and references therein. (b) D.M. Heinekey, C.E. Radzewich, Organometallics 17 (1998) 51.
[10] W.V. Konze, B.L. Scott, G.L. Kubas, Chem. Commun. (1999) 1807.
[11] (a) F. Calderazzo, G. Pampaloni, L. Rocchi, U. Englert, Organometallics 13 (1994) 2592. (b) I. Chávez, A. Alvarez-Carena, E. Molins, A. Roig, W. Maniukiewicz, A. Arancibia, H. Brand, J.M. Manríquez, J. Organomet. Chem. 601 (2000) 126.
[12] M. Tilset, G.S. Bodner, D.R. Senn, J.A. Gladysz, V.D. Parker, J. Am. Chem. Soc. 109 (1987) 7551.
[13] A.T. Patton, C.E. Strouse, C.B. Knobler, J.A. Gladysz, J. Am. Chem. Soc. 105 (1983) 5804.
[14] Leading references to isolable methylidene complexes: J.L. Brumaghim, G.S. Girolami, Chem. Commun. (1999) 953.
[15] S.R. Bahr, P. Boudjouk, J. Org. Chem. 57 (1992) 5545.
[16] J. Sandström, Dynamic NMR Spectrometry, London, Academic Press, 1982 Chapters 6–7.
[17] W. Weng, T. Bartik, M.T. Johnson, A.M. Arif, J.A. Gladysz, Organometallics 14 (1995) 889.
[18] (a) P.J. Hay, W.R. Wadt, J. Chem. Phys. 82 (1985) 299. (b) T.H. Dunning Jr., P.J. Hay, Modern Theoretical Chemistry, in: H.F. Scheafer III (Ed.), Plenum Press, New York, 1976. The double zeta basis set and a set of polarization function (DZp) for carbon (10s5p[3s/2p]721/41) with a polarization function ($\zeta = 0.6$) and for hydrogen (4s[2s]/31). For phosphorus the pseudopotential (3s/3p[2s/2p]21/21) with a set of polarization function ($\zeta = 0.6$). The basis set for rhenium required has the DZ quality {8s/6p/3d[3s/3p/2d]341/321/21) with ($\zeta = 0.073$), and the (n-1)s and (n-1)p electrons were considered as part of the valence space.
[19] GAUSSIAN-98, Revision A.5, M.J. Frisch, G.W. Trucks, H.B. Schlegel, G.E. Scuseria, M.A. Robb, J.R. Cheeseman, V.G. Zakrzewski, J.A. Montgomery Jr., R.E. Stratmann, J.C. Burant, S. Dapprich, J.M. Millam, A.D. Daniels, K.N. Kudin, M.C. Strain, O. Farkas, J. Tomasi, V. Barone, M. Cossi, R. Cammi, B. Mennucci, C. Pomelli, C. Adamo, S. Clifford, J. Ochterski, G.A. Petersson, P.Y. Ayala, Q. Cui, K. Morokuma, D.K. Malick, A.D. Rabuck, K. Raghavachari, J.B. Foresman, J. Cioslowski, J.V. Ortiz, B.B. Stefanov, G. Liu, A. Liashenko, P. Piskorz, I. Komaromi, R. Gomperts, R.L. Martin, D.J. Fox, T. Keith, M.A. Al-Laham, C.Y. Peng, A. Nanayakkara, C. Gonzalez, M. Challacombe, P.M.W. Gill, B. Johnson, W. Chen, M.W. Wong, J.L. Andres, C. Gonzalez, M. Head-Gordon, E.S. Replogle, J.A. Pople, Gaussian, Inc., Pittsburgh PA, 1998.

[20] For theory and applications: (a) W.J. Hehre, L. Radom, P.v.R. Schleyer, J.A. Pople, Ab Initio Molecular Orbital Theory, New York, 1986. (b) J.B. Foresman, Æ. Frisch, Exploring Chemistry with Electronic Structure Methods: A Guide to Using GAUSSIAN, Second Edition; Gaussian, Inc.: Pittsburgh PA, 1996.
[21] (a) NBO Program, 3.1, E.D. Glendening, A.E. Reed, J.E. Carpenter, F. Weinhold. (b) A.E. Reed, L.A. Curtiss, F. Weinhold, Chem. Rev. 88 (1988) 899.
[22] (a) W.A. Kiel, G.-Y. Lin, A.G. Constable, F.B. McCormick, C.E. Strouse, O. Eisenstein, J.A. Gladysz, J. Am. Chem. Soc. 104 (1982) 4865. (b) S. Georgiou, J.A. Gladysz, Tetrahedron 42 (1986) 1109.
[23] For other computational studies involving chiral rhenium complexes, see Ref. 7b and the following: (a) G.S. Bodner, A.T. Patton, D.E. Smith, S. Georgiou, W. Tam, W.-K. Wong, C.E. Strouse, J.A. Gladysz, Organometallics 6 (1987) 1954. (b) G.S. Bodner, D.E. Smith, W.G. Hatton, P.C. Heah, S. Georgiou, A.L. Rheingold, S.J. Geib, J.P. Hutchinson, J.A. Gladysz, J. Am. Chem. Soc. 109 (1987) 7688. (c) W.E. Buhro, B.D. Zwick, S. Georgiou, J.P. Hutchinson, J.A. Gladysz, J. Am. Chem. Soc. 110 (1988) 2427. (d) P.T. Czech, J.A. Gladysz, R.F. Fenske, Organometallics 8 (1989) 1806.
[24] R.F. Jordan, J.R. Norton, J. Am. Chem. Soc. 101 (1979) 4853.
[25] (a) F.B. McCormick, R.J. Angelici, R.A. Pickering, R.E. Wagner, R.A. Jacobson, Inorg. Chem. 20 (1981) 4108. (b) For metal–PPh_3 rotational barriers, see S.G. Davies, A.E. Derome, J.P. McNally, J. Am. Chem. Soc. 113 (1991) 2854, and references therein.
[26] W.A. Kiel, G.-Y. Lin, G.S. Bodner, J.A. Gladysz, J. Am. Chem. Soc. 105 (1983) 4958.
[27] L. Dahlenburg, A. Weiß, M. Bock, A. Zahl, J. Organomet. Chem. 541 (1997) 465.
[28] S.G. Davies, I.M. Dordor-Hedgecock, K.H. Sutton, M. Whittaker, J. Am. Chem. Soc. 109 (1987) 5711.
[29] A.G. Orpen, N.G. Connelly, J. Chem. Soc. Chem. Commun. (1985) 1310.
[30] H. Jiao, Unpublished computations, University Erlangen-Nürnberg.
[31] J.H. Merrifield, C.E. Strouse, J.A. Gladysz, Organometallics 1 (1982) 1204.
[32] T.-S. Peng, A.M. Arif, J.A. Gladysz, J. Chem. Soc. Dalton Trans. (1995) 1857.
[33] B.E.R. Schilling, R. Hoffmann, D.L. Lichtenberger, J. Am. Chem. Soc. 101 (1979) 585.
[34] A.K. Rappé, W.A. Goddard, III, J. Am. Chem. Soc. 99 (1977) 3966.
[35] G.L. Crocco, K.E. Lee, J.A. Gladysz, Organometallics 9 (1990) 2819.
[36] B.E.R. Schilling, R. Hoffmann, J.W. Faller, J. Am. Chem. Soc. 101 (1979) 592.
[37] H. Jiao, J.A. Gladysz, (in preparation).
[38] (a) J.W. Hershberger, R.J. Klingler, J.K. Kochi, J. Am. Chem. Soc. 105 (1983) 61. (b) N.N. Turaki, J.M. Huggins Organometallics 5 (1986) 1703. (c) Y. Huang, G.B. Carpenter, D.A. Sweigart, Y.K Chung, B.Y. Lee, Organometallics 14 (1995) 1423, and references therein.
[39] (a) D. Astruc, Acc. Chem. Res. 24 (1991) 36. (b) P. Legzdins, W.S. McNeil, M.J. Shaw, Organometallics 13 (1994) 562.
[40] G.S. Bodner, J.A. Gladysz, M.F. Nielsen, V.D. Parker, J. Am. Chem. Soc. 109 (1987) 1757.
[41] W.E. Meyer, A.J. Amoroso, C.R. Horn, M. Jaeger, J.A. Gladysz, submitted to Organometallics.
[42] M. Brookhart, B. Grant, A.F. Volpe, Jr., Organometallics 11 (1992) 3920.
[43] G.M. Sheldrick, SHELXL-93, University of Göttingen, Göttingen, Germany, 1993.